Soft Matter

PAPER

View Article Online
View Journal

Cite this: DOI: 10.1039/d0sm00932f

Collapse and cavitation during the drying of water-saturated PDMS sponges with closed porosity†

Phu Tuan Anh Nguyen,[ab] Matthieu Vandamme [a] and Artem Kovalenko *[b]

In this paper, we study the drying of water-saturated porous polydimethylsiloxane (PDMS) elastomers with closed porosity in which the evaporation of water is possible only *via* the diffusion across PDMS. Starting from water/PDMS emulsions, we fabricate soft macroporous samples with different pore diameter distributions and average diameters ranging from 10 to 300 μm. In these materials, the drying may lead to either a collapsed state with low porosity or the cavitation and reopening of a fraction of the pores. Using optical microscopy and porosity measurements, we showed the influence of the pore diameters and interactions on the result of drying. At pore diameters lower than 30 μm, the majority of pores remain collapsed. We attribute the permanence of the collapse of most small pores to a low probability of cavitation and to the adhesion of the pore walls. Pores with diameters larger than 100 μm reopen *via* cavitation of the water they contain. The behavior of pores with diameters ranging from 30 to 100 μm depends on the porosity and drying temperature. We also visualize collective cavitation upon the drying of sponges initially saturated with sodium chloride solution. In this case, the cavitation in the largest pores leads to the reopening of small pores in a neighboring zone of the sample. To our knowledge, our results present the first experimental proof of the pore-size-dependent and cooperative nature of the response of soft sponges with closed porosity to drying.

Received 20th May 2020,
Accepted 8th September 2020

DOI: 10.1039/d0sm00932f

rsc.li/soft-matter-journal

1. Introduction

Porous polymers are widely used for acoustic and thermal insulation. In recent years, increasing attention has been paid to soft porous elastomers, or sponges,[1] due to their use as compressible parts in mechanical sensors and soft actuators. Moreover, these materials were used to fabricate novel acoustic metamaterials[2] and gradient lenses[3] due to extremely low values of the sound speed obtained at ultrasound frequencies.[4] To achieve a controlled porous structure, a template consisting of liquid droplets[5] or solid particles[6] is dispersed in a liquid prepolymer, usually polydimethylsiloxane (PDMS), which is then crosslinked to obtain an elastomer. The template is then removed by etching[7] (in the case of solid particles), washing and drying to obtain pores with sizes and volume fraction similar to those of the template. Ideally, the drying step should lead to air-filled porous materials with low mechanical moduli. However, it was reported previously that capillary forces during drying may lead to a collapse of the porosity and to a loss of the desired acoustic or mechanical properties.[8,9] One solution to avoid this effect is to generate open porosity by using adhesive emulsions with an aggregated droplet structure.[9] The micron-sized "windows" between pores allow water evaporation and air invasion in the pores. This method suffers from the sensitivity to the emulsion fabrication conditions and the spatial inhomogeneity of the aggregated porous structure. The second strategy is to use supercritical drying.[3,8] This approach requires consecutive washing of the samples with an intermediate solvent (for example, ethanol) and liquid carbon dioxide which is then removed *via* a supercritical cycle at high pressure. While it allows the fabrication of materials with closed porosity and microscopically homogeneous pore distribution, such a process is expensive and time-consuming. Thus, it would be interesting to propose alternative approaches of drying for soft sponges with closed, homogeneously distributed porosity, which is impossible without the rationalization of the collapse problem. However, neither the collapse mechanism during thermal drying nor the dependence of the final porosity on material parameters and drying conditions is yet well understood.

Interestingly, Milner *et al.*[10] have recently shown that an "isolated" water-filled pore in PDMS with diameter $d \sim 1$ mm reopens during drying *via* cavitation (*i.e.*, *via* the formation of a

[a] Navier, Ecole des Ponts, Univ. Gustave Eiffel, CNRS, Marne-la-Vallée, France
[b] Laboratoire Sciences et Ingénierie de la Matière Molle, ESPCI Paris, PSL University, Sorbonne Université, CNRS, F-75005 Paris, France. E-mail: artem.kovalenko@espci.fr

† Electronic supplementary information (ESI) available. See DOI: 10.1039/d0sm00932f

bubble inside the water it contains). The authors observed the shape of the pore and showed the presence of several drying stages. In the first so-called "breathing" mode, the pore contracted homogeneously and remained spherical. Next, a creasing instability was observed on the pore surface which led to a non-spherical pore shape. According to Cai *et al.*,[11] this instability is preferred to buckling for thick pore walls (corresponding to low porosities for sponges). The number of creases depends on the surface energy of the pore and on the high-strain mechanical properties of the elastomer. The next drying stage which takes place at a certain moment before or after creasing is the cavitation of the water it contains[10,12] (*i.e.* the nucleation of a water vapor bubble). This stage is followed by the release of the (negative) pressure inside the pore and by an expansion of the pore back to its initial size and shape. By tackling the bubble expansion velocity during this last stage, Bruning *et al.* estimated[12] the cavitation pressure $p_{cav} \approx -1.4$ MPa, the absolute value of which is much lower than 20–30 MPa found for water in rigid monodisperse pores by Vincent *et al.*[13] and synthetic trees by Wheeler *et al.*[14] This difference was explained by the highly hydrophobic nature of PDMS which favors heterogeneous bubble nucleation.

Cavitation is the necessary but not sufficient condition for pore reopening. The stress in the matrix should be high enough to promote the cavity growth. This effect was intensively investigated in the literature related to such cavity growth in adhesives and elastomers,[15] which is also called "cavitation" although no liquid is involved. We will refer to this process as "solid cavitation", to avoid any ambiguity with the cavitation of the pore water in water-saturated porous solids, which was described in the previous paragraph. It was shown that a small pore inside an elastic matrix with Young's modulus E is unstable and will grow to an infinite size at mean tensile stresses higher than $5/6E$: such dependence of the stress at which "solid cavitation" occurs on the modulus was observed experimentally.[15–17] For the analysis of the stability of small pores, the polymer surface energy should be taken into account. Gent and Tompkins[16] introduced the surface energy term in the mechanical model of pore deformation. They showed that the critical mean stress for the infinite inflation of the pore increases with a decreasing initial radius of this pore and attains hundreds of MPa for a radius of a few nanometers. The characteristic length scale of the action of surface forces is called the elasto-adhesive length γ/E, where γ is the surface energy of the elastomer. For a typical PDMS elastomer with γ = 40 mN m^{-1} and $E \sim 1$ MPa, the elasto-adhesive length is 0.04 μm. The model of Gent and Tomkins shows that a significant impact of surface energy on the tensile stress at which pore growth occurs is observed for pore dimensions lower than 0.1 μm.[16,17] For larger cavities, the growth should be observed at stresses of the order of the modulus E, *i.e.* about 1 MPa. This explains why the individual large pores in PDMS observed by Milner *et al.*[10] and Bruning *et al.*[12] reopen after cavitation at $p_{cav} \approx -1.4$ MPa.

The aim of this study is to characterize experimentally the effect of the size and number of pores on how porous elastomers with closed porosity initially saturated with water or a salt solution behave during drying. Using previously reported emulsion-templated protocols,[4] we synthesize macroporous polydimethylsiloxane (PDMS) with pore diameters ranging from 1 to 100 μm. First, we use optical microscopy to observe the drying of "diluted" pores (5% porosity) in thin (*i.e.* with a 0.5 mm thickness) water-saturated samples. We show that the pore behavior differs regarding their diameters: after their total shrinkage, pores with diameters larger than 30 μm are most likely to reopen *via* cavitation while the majority of smaller pores remain in a collapsed state for at least 16 hours of observation. The part of reopened pores increases with increasing the drying temperature from 60 °C to 110 °C. Next, by using density measurements to measure porosity, we compare the drying of thick (*i.e.*, with a thickness of about 10 mm) water-saturated samples with 30% porosity and two different pore size distributions. After drying, the sample with small pores ($d \sim 70$ μm) is almost completely collapsed while the sample with larger pores ($d \sim 300$ μm) shows reopening of a significant fraction of its pores. Finally, we show the cooperative nature of the cavitation of pores in samples initially containing sodium chloride solution in the pores. We observe that the opening of larger pores leads to the reopening of neighboring small pores. To our knowledge, the observed size-dependent and cooperative effects were not reported before and present an interest for soft matter physics.

2. Experimental

2.1. Materials

A two-component Sylgard® 184 PDMS kit was supplied by Neyco. It is composed of the vinyl-modified PDMS base (SiVi) and the silane-modified PDMS curing agent (SiH). We used deionized Milli-Q water and NaCl from Sigma-Aldrich.

2.2. Synthesis of porous PDMS samples

We used the previously reported emulsion-templated method of synthesis.[4] The continuous phase of the emulsions was obtained by mixing the SiVi and SiH parts in a 10 : 1 ratio. After mixing, the continuous phase was degassed at room temperature to remove bubbles. The water phase was either Milli-Q water or a 1.5 wt% NaCl solution. Surprisingly, stable emulsions with a 5% or 30% volume fraction of water could be produced without adding any surfactant. We explain this by the high viscosity of PDMS and the presence of low-molecular species[18] that can act as surfactants. The corresponding amount of water was incorporated into about 40 g of PDMS under gentle mixing with a spatula (at approximately 1 tour per second). The mixture was then stirred for 2 minutes *via* a Heidolph RZR 2162 mechanical mixer with a helical geometry with a diameter of 3 cm. The stirring conditions are given in Table 1.

By controlling the stirring speed of the emulsions and, consequently, the shear stress, one should be able to tune the size of the droplets. However, because of the high viscosity of Sylgard 184, it was impossible to obtain narrow size distributions

Table 1 Characteristics and drying investigation methods of the fabricated sponges

Sample name	Initial porosity (%)	Stirring speed (rpm)	Volume-weighted mean pore diameter (μm)	Aqueous phase	Optical microscopy (thin samples)	Porosity measurements (thick samples)
D200-5	5	375	200	Milli-Q water	+	−
D10-5	5	1500	10	Milli-Q water	+	−
D300-5NaCl	5	375	300	1.5% NaCl	+	−
D50-5NaCl	5	800	50	3.65% NaCl	+	−
D300-30	30	200	300	Milli-Q water	−	+
D70-30	30	375	70	Milli-Q water	−	+

using simple mixing devices. After several tests, we determined empirically stirring protocols giving samples with significantly different drying properties. The pore diameter distributions $N_i(d_i)$ were obtained *via* manual pore tracking of optical microscopy images on at least 1000 pores using ImageJ software. The pore distribution by volume $\varphi_i(d_i)$ was calculated using the equation:

$$\varphi_i(d_i) = \frac{N_i d_i^3}{\sum_i N_i d_i^3} \quad (1)$$

where N_i is the number of pores with diameter d_i.

To obtain samples for microscopy, the volume fraction of the aqueous phase was fixed at 5%. The emulsion was then poured between two PET-coated glass molds with a 0.5 mm rubber spacer and the molds were placed in a sealed metallic box and heated at 60 °C for 14 hours. These samples are designated as ''thin'' in the rest of the paper.

For density measurements, we fabricated samples starting from a 30% emulsion. The emulsion was poured in 60 mL plastic tubes and centrifuged at 1000 rpm for 5 min to remove gas bubbles. After polymerization at 60 °C for 14 hours, the samples were unmolded and cut into equivalent pieces with an average weight of 5 g and a thickness of about 10 mm. These samples are designated as ''thick'' in the rest of the paper.

In Table 1 we summarize the composition, stirring conditions and mean pore diameters for the samples and the methods we used to study their drying.

2.3. Observation of the drying of thin samples with 5% porosity

The samples with 5% initial porosity and a thickness of 0.5 mm were placed in an HFS 91 heating microscope stage (Linkam) under an optical microscope. The cell was connected to an air pump which maintained a flow of dry air equal to 0.5 liters per min through the chamber. After rapid heating to the desired temperature (for about 1 min), the recording of images was performed every 10–30 s using a ×10 objective. Two drying temperatures, 60 °C and 110 °C, were used for each sample. The drying of sample D200-5 was also performed at 90 °C.

2.4. Drying and characterization of thick samples with 30% porosity

For thick samples (about 10 mm thickness), we desired to perform the drying at a well-controlled temperature and without any solid support which could create tangential stress affecting the shrinkage of the sample. Thus, the drying was done in hot glycerol which homogenizes rapidly the temperature and does not diffuse into the pores (and hence does not swell the matrix). A 50 mL vial was filled with dry glycerol and heated to the desired drying temperature. Next, the sample was immerged in the bath for 7 days. This time was enough for complete drying, as deduced from the fact that the relative weight loss reached an asymptotic value close to the initial water mass fraction, with the difference between the relative weight losses at the 7th and 8th days being less than 0.2%. The initial porosity of the samples was calculated from the amount of water lost during drying. Similar values, very close to 30%, were obtained for specimens extracted from the top and from the bottom of the centrifugation tube. Thus, we concluded that centrifugation did not create measurable gradients in the volume fraction of the emulsion.

The density of the dried samples was measured by using a home-made hydrostatic balance which measures the force necessary to immerge a sample in a liquid using a thin rigid wire. To increase the precision, we used several liquids including pure water and NaCl solution with concentrations ranging from 3 to 7 wt%. The density was calculated using the balance of the forces acting on the immerged sample:

$$m_{\text{sample}} + \Delta m_{\text{pull}} = \rho_{\text{liquid}} V_{\text{sample}} \quad (2)$$

We thus infer:

$$\frac{\Delta m_{\text{pull}}}{m_{\text{sample}}} = \frac{\rho_{\text{liquid}}}{\rho_{\text{sample}}} - 1 \quad (3)$$

where m_{sample}, V_{sample} and $\rho_{\text{sample}} = m_{\text{sample}}/V_{\text{sample}}$ are the mass, volume, and mass density of the sample, respectively; ρ_{liquid} is the mass density of the liquid and Δm_{pull} is the difference between the mass measured when the sample is forcibly immerged in the liquid by plunging the thin rigid wire and the mass measured in the absence of the sample but when the thin rigid wire is plunged in an identical position. The sample density was obtained from an affine fit of the curve of $\Delta m_{\text{pull}}/m_{\text{sample}}$ as a function of ρ_{liquid}, since, as eqn (3) shows, the slope of this fit must be equal to $1/\rho_{\text{liquid}}$ (the curves are shown in SI-1a, ESI†). By using the same method, we measured the density of the PDMS matrix $\rho_{\text{PDMS}} = 1034$ kg m^{-3}, which is slightly lower than the reported value[18] of 1100 kg m^{-3}. To calculate the sample porosity $\Phi = V_{\text{pores}}/V_{\text{sample}}$ (where V_{pores} is the volume of pores in the sample), we used the following equation:

$$\Phi = 100\% \times \left(1 - \frac{\rho_{\text{sample}}}{\rho_{\text{PDMS}}}\right) \quad (4)$$

2.5. Other characterizations

The microstructures of the obtained porous samples were characterized with a TM-1000 scanning electron microscope (Hitachi). Prior to imaging, the samples were fractured in liquid nitrogen, dried at 60 °C and covered with a thin gold layer by vapor deposition. The observation was performed on the fractured surface.

Tensile loading measurements on parallelepipedal samples about 30 × 5 × 0.5 mm^3 in size were performed using Instron 5565 apparatus. In the linear elastic regime, the dependence of the axial force F on the axial strain ε was obtained and treated according to Hooke's law:

$$\sigma = E\varepsilon \quad (5)$$

where $\sigma = F/S$ is the axial stress, S is the initial cross-section area of the sample, and $\varepsilon = (L - L_0)/L_0$ with L_0 and L being the length of the sample before and during the test, respectively.

3. Results and discussion

3.1. Structure and mechanical properties of the PDMS sponges

For both the synthesized samples with 5% and 30% of the dispersed water (or salt solution) phase, the porosity is closed. This is confirmed by the electronic microscopy images of the sample sections shown in Fig. 1a and b. The fact that the pores are less spherical than those on the optical microscopy images (see the next sections) may be due to the cutting- and drying-induced stresses. The closed porosity is formed because of the isolated droplet structure of the emulsion;[9] moreover, at 5% and 30% of porosity, the pore walls are rather thick and are not connected by macroscopic windows between them. As in the case of a unique water-filled pore,[10] the drying of such samples occurs by pervaporation through PDMS and not by the invasion of the pore network by a liquid–vapor meniscus.

We also checked that the macroscopic mechanical properties of water-filled porous samples are qualitatively similar to those of the non-porous PDMS, as confirmed by the stress–strain curves shown in Fig. 1c, which exhibits curves with a similar shape. The Young's modulus of the wet non-porous PDMS is about 1.6 MPa and decreases to 1.16 MPa and 0.98 MPa for water-saturated porous samples with porosities equal to 5% and 30%, respectively. The decrease of modulus for the water-saturated porous samples with respect to the dry bulk PDMS may be explained by the presence of pores and by the influence of humidity on polymerization. The fact that the difference in modulus between the wet non-porous PDMS and any of the two water-saturated porous samples is larger than that between the two water-saturated porous samples suggests that, for our samples, the modulus is more significantly impacted by humidity than by the presence of pores. Water may hydrolyze some of the Si–H groups in the curing agent and decrease the degree of curing.[19] However, the effect is minor and should not drastically impact the interpretation of the results in the next sections.

3.2. Visualization of the pore collapse and reopening

First, we performed a microscopic observation of the drying of sample D200-5 with 5% porosity and very polydisperse pore diameter distribution (red bars in Fig. 2a and b). The corresponding optical microscopy image in the initial water-saturated state is shown in Fig. 2c. When counting by number, the distribution is centered at about 20 μm; however, the volume-weighted distribution obtained *via* eqn (1) is centered at about 200 μm. The volume-weighted distribution is more relevant for the porosity Φ which is, by definition, the volume fraction of pores.

Fig. 2d–f show the microscopy images of pores in sample D200-5 when dried at 110 °C. For a video-stack of drying images, see SI-2 (ESI†). First, we observe a rapid shrinkage of small pores which seem to disappear (Fig. 2d). The pores with larger diameters also decrease in volume and show a transition to a creased state, as observed for the central pore shown in Fig. 2e. We define the time of collapse as the moment when pores are non-detectable. For larger pores the dissolution time is longer. This may be explained with the diffusive model of the pore shrinkage proposed by Milner *et al.*[10] and Bruning *et al.*[12] In this model, the diameter of the pore scales with time t as $d = d_0\sqrt{1 - kt/d_0^2}$ where d_0 is the initial diameter and the kinetic factor k is mainly governed by the diffusion coefficient and the difference between the water concentration c_{eq} in PDMS near the pore and c_∞ near the edge of the sample. In the absence of impurities (such as salt), the values of c_{eq} and the diffusion coefficient depend only on temperature. The concentration c_∞ on the edge of the sample is determined by the relative humidity in the chamber. Hence, we may suppose

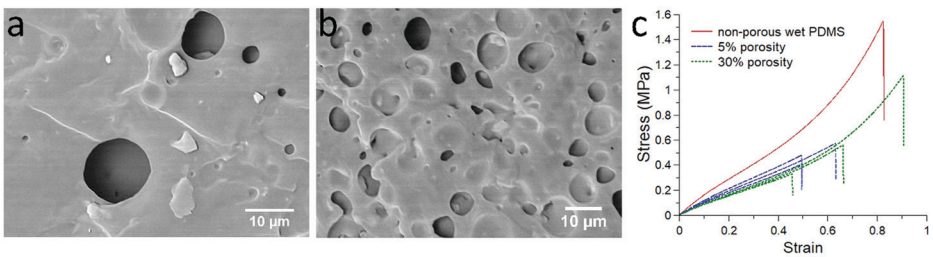

Fig. 1 (a and b) Scanning electron microscopy images of the sections of sample D200-5 with 5% porosity (a) and sample D70-30 with 30% porosity (b). (c) Stress–strain curves of the same samples in the wet state in comparison with non-porous PDMS "swollen" in water at 60 °C for 6 hours (red curve). For each type of porous sample, the measurement was performed on 3 samples.

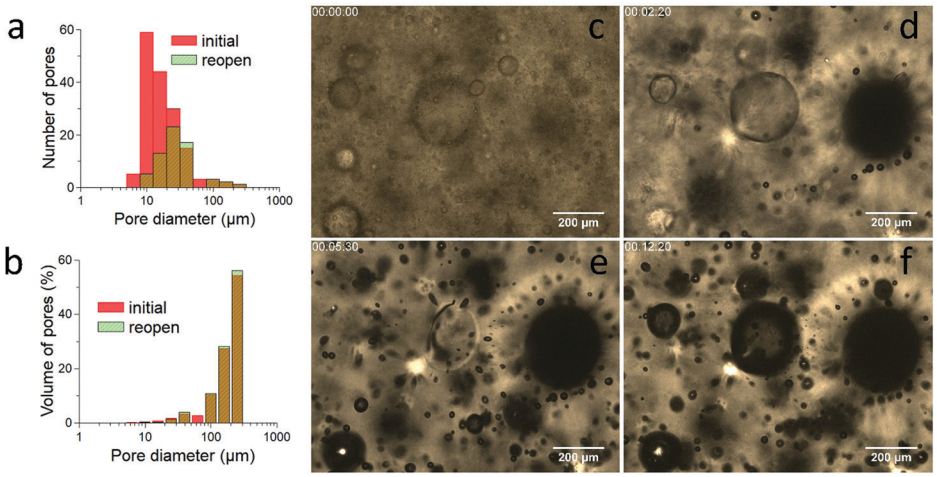

Fig. 2 (a and b) Distributions of pore diameters in sample D200-5 obtained for initial, water-filled pores (red) and pores reopened *via* cavitation (semi-transparent green); (c–f) optical microscopy images of sample D200-5 during drying at 110 °C. The overlap of the pore diameter distributions between water-filled and reopened pores is indicated in brown.

the value of k to be similar for all pores. The dissolution time scales as $t_{\mathrm{collapse}} \sim {d_0}^2$, which explains the fact that the small pores reach full shrinkage faster compared to the large pores. However, a quantitative analysis of the porous sample would not be straightforward because the model was developed for a single pore and does not include interactions between pores with different drying dynamics.

Some pores reopen *via* cavitation, giving pores of diameters similar to the initial ones and located at places similar to the initial ones (compare the final state in Fig. 2f and the initial state in Fig. 2c). The reopened pores show a higher contrast than in the water-saturated state because of the difference of the optical index between PDMS and water vapor. As shown in Fig. 2a, the comparison between the diameter distribution of the reopened pores and that of the pores before drying shows that most pores with diameters lower than 30 μm remain collapsed while the majority of larger pores reopen. However, in the case of the volume-weighted diameter distribution (Fig. 2b), the contribution of the small pores is almost invisible, meaning that their collapse will not strongly affect the total pore volume and hence the porosity. The fact that the number of reopened pores with a diameter around 40–50 μm is higher than the number of pores observed before drying may be caused by the change of the transparency of the sample during drying, because of which deeper pores may become visible. Because of the small pore size, the optical microscopy does not allow a precise determination of the nature of the cavitation (liquid or "solid" one). The results reported by Bruning *et al.*[12] on millimeter-scale pores in PDMS demonstrate that the cavitation occurs in the water phase and the pore reopening happens about 0.1 ms after the cavitation. We did not observe any correlation between different cavitation events: reopening happened some time after the complete shrinkage of a given pore, with no obvious trend.

For a second experiment, we chose sample D10-5 which contains exclusively small pores (Fig. 3a) with an average diameter of about 10 μm (the diameter distribution was obtained from the image of a thin layer of the emulsion used for the synthesis shown in SI-1b, ESI†). In this case, the imaging of pores is very challenging because of their small diameters and the change of the transmittance of the sample with time (see the video-stack of drying images in SI-3, ESI†). However, once the pores reopen, their detection is quite easy. Only pores that were located near the focus plane and that appeared as black spots were counted as reopened. First, we performed a drying procedure at 60 °C, far below the boiling point of water. The images show that most pores remain collapsed and invisible in the shrunk state while only a few pores reopen (Fig. 3b). In the present configuration of the microscope, the effective depth of field (DOF), *i.e.* the distance which allows

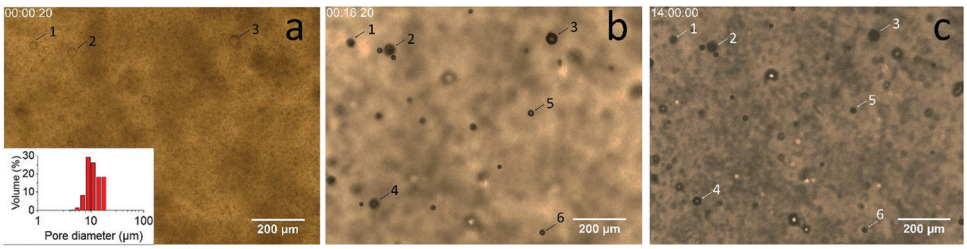

Fig. 3 Optical microscopy images of sample D10-5 during drying at 60 °C: (a) initial state (small pores are poorly visible); (b) state after 16 min of drying; and (c) state after 16 hours of drying. The inset in image (a) shows the pore diameter distribution in the initial state. Some clearly identified pores are labeled with numbers.

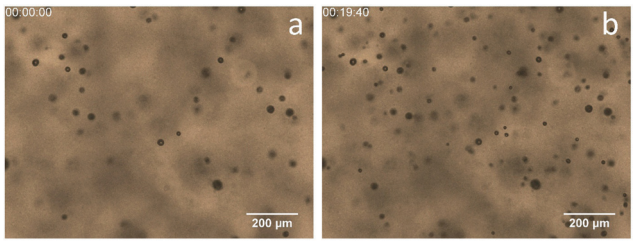

Fig. 4 Optical microscopy images of the same area in sample D10-5 before (a) and after (b) increasing the drying temperature from 60 °C to 110 °C.

simultaneous detection of the reopened pores, was roughly estimated by changing the focus distance as DOF ∼ 200 μm. Taking the image with lateral dimensions $H \times W = 1200 \times 900\ \mu m^2$, we assumed that pores are spherical and calculated the volume of the reopened pores $V_{pores}^{60°C} \approx 3 \times 10^5\ \mu m^3$. The porosity is therefore estimated as $\Phi^{60°C} \approx V_{pores}^{60°C}/(DOF \times H \times W) \approx 0.15\%$. This value is at least one order of magnitude lower than the initial porosity equal to 5%. This confirms that the majority of the pores collapsed and did not reopen. The number of reopened pores does not change after 30 min of drying for at least 16 hours (Fig. 3c). The background on the image at 16 hours appears darker and less homogeneous because of the low light intensity used to acquire this image. We also show the images of initial and dry states at a higher magnification in SI-1c (ESI†).

Sample D10-5 dried for 16 hours at 60 °C was next heated to 110 °C, which is above the boiling temperature of water. Fig. 4 and SI-4 (ESI†) show that heating led to the reopening of another small fraction of pores. Following the same methodology as at 60 °C, the final porosity at 110 °C may be estimated at about 0.3%, which is well below the initial one. This analysis confirms that small pores remain shrunk at least until the end of the experiment.

3.3. Macroscopic porosity measurements

We compare samples D70-30 and D300-30 which have similar initial porosity $\Phi_{init} \approx 30\%$ and different pore sizes. Fig. 5 shows the optical images of a cross-section of the samples. The number-weighted distributions as well as some additional images are shown in SI-1d (ESI†). In contrast to the transparent samples with 5% porosity (Section 3.2), the samples are opaque and the observation of the pores is possible only near the cross-section plane. The probability of a pore to be found in the cross-section is inversely proportional to its diameter[20] and thus $N_i \propto N_i^{section}/d_i$, where $N_i^{section}$ is the number of pores with diameter d_i observed in the cross-section and N_i are the number of pores with diameter d_i in the sample. Consequently, the volume fraction φ_i of pores with diameter d_i is given by

$$\varphi_i(d_i) = \frac{N_i d_i^3}{\sum_i N_i d_i^3} = \frac{N_i^{section} d_i^2}{\sum_i N_i^{section} d_i^2}. \quad (6)$$

The obtained distributions are displayed in Fig. 5c.

The data of the samples dried in a glycerol bath at 60 °C or 110 °C are presented in Fig. 6a. For both temperatures, the drying loss (which is equal to the ratio between the total volume of evaporated water and the initial volume of the sample, which is therefore an estimate of the initial porosity) was about 30%. Next, we show the porosity values calculated from the density data obtained using the hydrostatic balance. The porosity of sample D70-30 after drying is very low, which slightly increases with drying temperature from 0.5 to 3%. In contrast, sample D300-30 shows the reopening of almost a half of the pores (by volume). Again, the porosity increases with the drying temperature. The difference between the two samples is demonstrated by the flotation test in water shown in Fig. 6b: the porous sample D300-30 rapidly rises to the surface while the collapsed sample D70-30 sinks. Note that we did not detect any change in the porosity after several months of storage at room temperature.

3.4. Factors affecting the probability of reopening

The results of microscopy (Section 3.2) and macroscopic density measurements (Section 3.3) confirm that the pores with larger diameters are more likely to cavitate and reopen compared to small pores. Because of the large pore size distribution, it is difficult to demonstrate the existence of a critical pore diameter above which pores would reopen and below which pores would not. Also, we may expect the cavitation to be probabilistic and to depend not only on the pore diameter but also on small deviations of the pore shape and on the proximity to the neighboring pores.

We repeated the drying several times on different pieces of sample D200-5 at temperatures of 110 °C and 90 °C to obtain a statistically relevant measurement of the fraction of pores of a given diameter that reopen during drying. The results observed

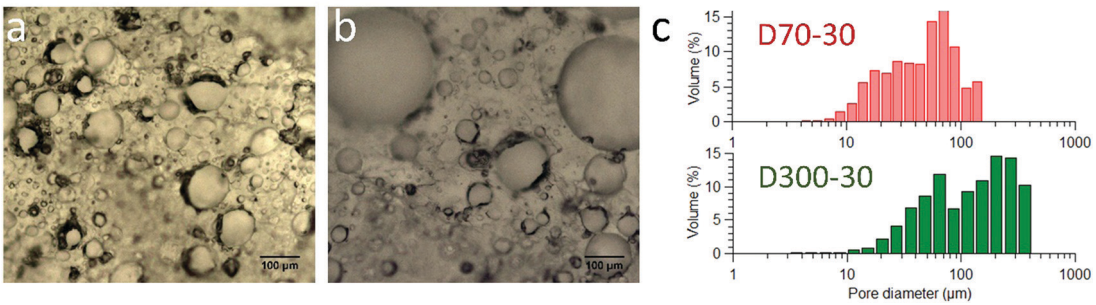

Fig. 5 Optical microscopy images of a cross-section of samples D70-30 (a) and D300-30 (b) and the corresponding volume-weighted diameter distributions (c).

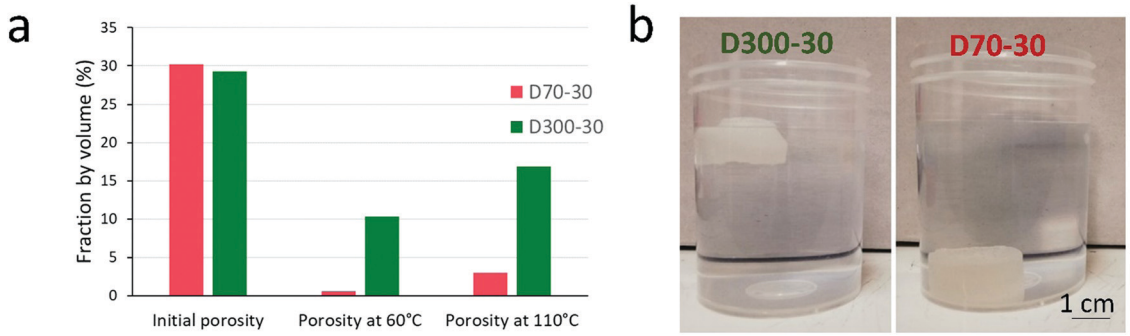

Fig. 6 (a) Characteristics of the dried thick samples with different pore sizes; (b) a photograph of the dried samples demonstrating flotation (D300-30) and sinking (D70-30) in pure water.

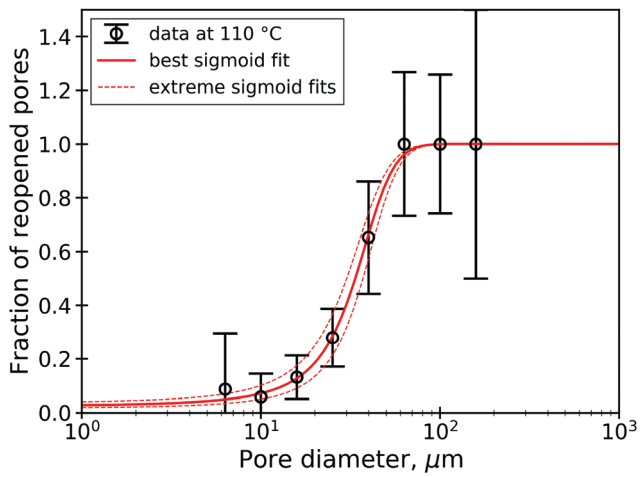

Fig. 7 Fraction of pores in sample D200-5 that reopened after drying at 110 °C. The data are obtained by adding results on 4 specimens. The parameters of the fitted sigmoidal function are d_{char} = 33.6 ± 3.5 μm and p = 4.0 μm. The error bars are obtained as $1/\sqrt{N_i}$, where N_i is the number of pores with diameter d_i filled with water. The error in the fitted value of d_{char} is estimated by determining the extreme values of d_{char} that make it still possible for the fitted sigmoidal function to remain in the experimental uncertainty.

at 110 °C are displayed in Fig. 7. The results obtained at 90 °C are very similar and are shown in SI-1e (ESI†). We observe that, mostly, the larger a pore, the more likely it is to reopen. We fitted a sigmoid function of the form $1/(1 + \exp(-(d - d_{char})/p))$ to these experimental data, where d_{char} is a characteristic diameter and p is a characteristic standard deviation. A least-squares fit yielded d_{char} = 33.6 ± 3.5 μm and p = 4.0 μm. Above d_{char}, the pores tend to reopen during drying, and below d_{char} they tend to remain closed during drying. A fit of the same function to the data at 90 °C yielded d_{char} = 26.0 ± 2.0 μm and p = 5.1 μm.

We now perform some hypothesis testing, by assuming that, in samples D300-30 and D70-30, the likelihood for a pore of a given diameter to reopen during drying at 110 °C is the same as that for sample D200-5 and is therefore given by the sigmoidal function $F(d_i)$ displayed in Fig. 7. We use the number-weighted distribution of pore diameters displayed in SI-1d (ESI†), obtained from the cross-sections of samples D300-30 and D70-30. Similarly to the derivation of eqn (6), the probability of finding the pores in the cross-section is inversely proportional to the pore diameter. Once all pores that are likely to reopen *via* cavitation have reopened, the number of reopened pores of diameter d_i must be equal to $F(d_i)N_i^{section}$, so that we can estimate the porosity Φ_{reopen} that the samples should have recovered during drying:

$$\Phi_{reopen} = \Phi_{initial} \frac{\sum_i F(d_i) N_i^{section} d_i^2}{\sum_i N_i^{section} d_i^2} \quad (7)$$

The initial porosity of both samples D300-30 and D70-30 was $\Phi_{initial}$ = 30%. Using eqn (7), we estimate that, after drying at 110 °C, the porosity of those 2 samples should be Φ_{reopen} = 26% and Φ_{reopen} = 19%, while the results displayed in Fig. 6a show that the porosities of those 2 samples are only 3% and 17%, respectively. Therefore, we can conclude that the probability for pores to reopen after drying at 110 °C is not the same for samples D300-30 and D70-30 as for sample D200-5. Consequently, this probability must not depend on the pore diameter only, but could depend also in particular on the porosity, since the initial porosity $\Phi_{initial}$ is the main difference between samples D300-30 and D200-5.

We now assume that, as for sample D200-5, there exist, for samples D300-30 and D70-30, characteristic sizes $d_{char}^{D300\text{-}30}$ and $d_{char}^{D70\text{-}30}$, respectively, above which pores tend to reopen during drying and below which pores tend to remain closed during drying. Using eqn (7) and the data of pore diameter distributions for samples D300-30 and D70-30, we find that correct predictions of the porosity after drying are obtained for $d_{char}^{D300\text{-}30} \sim$ 100–120 μm and $d_{char}^{D70\text{-}30} \sim$ 100–120 μm. This characteristic size is quite similar for samples D300-30 and D70-30 and therefore seems to not be impacted much by the mean diameter of the pores in the sample. This characteristic size is much larger than the one measured on sample D300-5, namely 34 μm. Consequently, we infer that the characteristic size (separating the larger pores that tend to reopen during drying from the smaller ones that tend to remain closed during the same drying) depends, for a given temperature of drying, on the porosity. Note that it could also depend on the mechanical properties of the solid skeleton or on the size of the sample (which impacts the kinetics of drying). The dependence of the

characteristic size on the porosity may be due to the fact that the effective elastic modulus of the medium decreases with increasing porosity. Indeed, we previously observed[9] a strong effect of porosity on the modulus of air-filled porous PDMS, *i.e.* a decrease by a factor of ~ 3 of the modulus of a sample with $\Phi = 30\%$ with respect to the non-porous one.‡ We thus may hypothesize that, after the reopening of one part of the porosity in samples D300-30 and D70-30, pores that are still collapsed behave as if they are surrounded by an effective medium with a much lower mechanical modulus, and hence the likelihood for those still-collapsed pores to reopen is significantly decreased. It is therefore possible that the characteristic size depends on the porosity as a consequence of its dependence on the elastic modulus of the medium.

Our observations do not allow the mechanism of pore collapse and reopening to be established. In accordance with the paper of Bruning *et al.*,[12] we may expect that the condition necessary for cavitation in a water-filled pore should be that the (negative) pressure reaches a threshold value of about −1.5 MPa. The existence of such a threshold value, which is independent of the size of the pore, does not explain directly the pore size dependence of the pore reopening that we observed. However, since the cavitation of water is a probabilistic process, one could argue that cavitation is more likely to happen in larger pores (which contain a larger amount of water) than in smaller pores, which would be in agreement with our experimental observations. The fact that the likelihood of cavitation increases with temperature[13] would also be in agreement with our experimental observations. The second condition for pore reopening is that the tensile stresses that prevail at the location of the collapsed pore after the cavitation of the fluid it contains has occurred should be high enough to allow the pore to reopen, akin to what is observed for "solid" cavitation (following the denomination that we used in the introduction). For small pores with $d < 0.1$ μm, the threshold tensile stress[16,17] for the growth of the pore may be much higher (in absolute value) than Young's modulus $E = 1.6$ MPa (which provides an order of magnitude of the tensile stresses that must prevail at the location of the collapsed pore). If we assume that the cavitation takes place in the water inside pores after they shrink to a diameter $d < 0.1$ μm, the surface energy may prevent the pore from reopening after the cavitation occurred. This would explain the dependence of the cavitation on the pore diameter. However, it is difficult to directly correlate the size and shape of an initially spherical pore in a highly deformed state with its initial size.

3.5. Drying in the presence of NaCl

In this section, we present microscopy observations during the drying of samples which contain NaCl salt solution inside pores. Due to its hydrophobic nature, PDMS is impermeable to the salt.[21] Thus, drying leads to the concentration of the NaCl solution and the crystallization of the salt inside the pores. The general image of drying is similar to the case without salt. However, a detailed investigation of the pore reopening shows the presence of cooperative effects.

Fig. 8 shows the optical images of sample D300-5NaCl in which the pores are filled with a 1.5 wt% NaCl solution. For a video-stack of drying images, see Fig. SI-5 (ESI†). The drying was performed at 110 °C. First, the pores shrink (Fig. 8a and b), similarly to what was observed without salt (Fig. 2c–f). No cavitation is observed during the first 6 minutes of drying. Next, a cluster of pores reopens simultaneously in the area labeled "a" (Fig. 8c). In the following 6 minutes, no new cavitation events happen. Next, a new cluster reopens simultaneously in the area labeled "b" (Fig. 8d). Similar qualitative features are observed for sample D50-5NaCl (whose pores are smaller than those of sample D300-5NaCl and filled with a 3.65% NaCl solution), for which the results are presented in Fig. 9. Again, the pore reopening happens by clusters of pores (see also SI-6 and 1f, ESI†). Interestingly, in the center of the clusters we observe the largest pores and the diameter of the cluster is about 2–3 times the diameter of these largest pores.

Fig. 10a displays the diameter of some pores in cluster "b" from Fig. 8 *versus* the drying time. After creasing of the pore surface, we are no longer able to measure the pore diameter; however, the time points at which reopening occurs (which is indicated with star symbols in the figure) are clearly detected due to a good contrast of the vapor-filled pores. The dashed lines on Fig. 10 indicate a linear extrapolation of the diameter evolution after creasing. While the collapse of small pores ("b2", "b3" and "b4") is expected to occur earlier than that of the large one ("b1"), we observe simultaneous reopening at about 900 s. Therefore, the reopening seems to be limited by the full shrinkage of the largest pore "b1". To better visualize

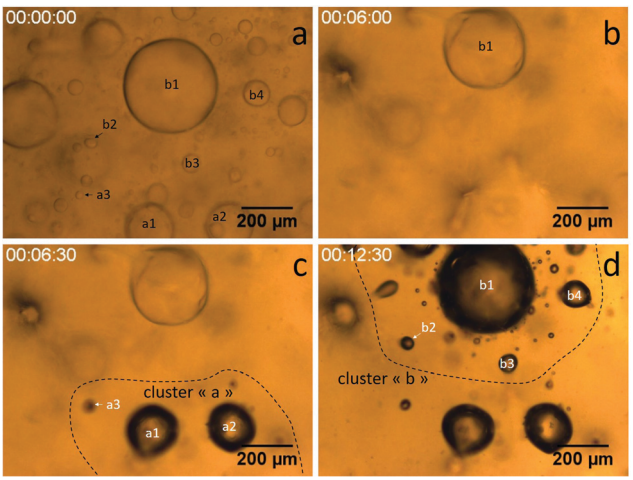

Fig. 8 Optical microscopy images of different drying stages of the porous PDMS sample with 5% porosity at 110 °C. Symbols a1–a3 and b1–b4 mark similar pores in pore clusters "a" and "b", respectively, before and after cavitation.

‡ In the present manuscript, we measured a Young's modulus of wet samples with $\Phi = 30\%$ which is only slightly lower than that of wet samples with $\Phi = 5\%$ (0.98 MPa and 1.16 MPa, respectively), but such low effect of the porosity is due to the fact that, in our experiments, pores are filled with liquid water, whose bulk stiffness is very high (*i.e.* around 2 GPa).

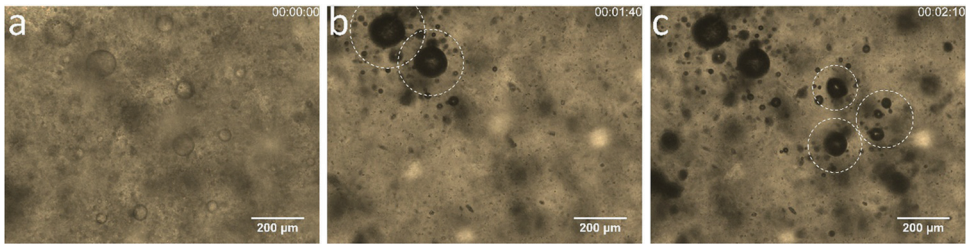

Fig. 9 Optical microscopy images showing the reopening pore clusters during the drying of sample D50-5NaCl at 110 °C.

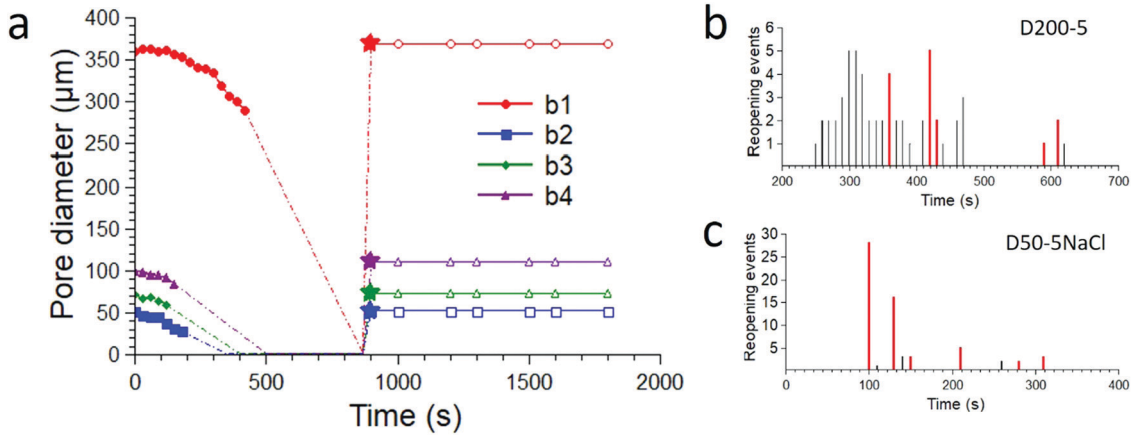

Fig. 10 (a) Evolution of the pore diameter before (filled symbols) and after cavitation (open symbols) for the pores from cluster "b" shown in Fig. 8. The points represent the data obtained when the pores had a well-defined ellipsoidal shape and were located close to the focal plane of the microscope. The supposed evolution of pore diameters after creasing instability or after eventual displacement out of the focus is represented by dashed lines to guide the eye. The moments at which reopening occurs are indicated with star symbols. (b and c) Number of cavitation events as a function of drying time at 110 °C for samples D200-5 (b) and D50-5NaCl (c). Red bars correspond to the reopening events of at least one pore with a diameter >50 µm.

this effect, we compare the reopening event statistics of samples D200-5 and D50-5NaCl in Fig. 10b and c. Both samples contain statistically significant numbers of pores with diameters in the 10–100 µm range. The vertical bars correspond to the number of reopened pores between two imaging frames (about 10 s). Red bars show the events including at least one "large" pore with diameter >50 µm. The comparison shows that, in the case of D200-5, many small pores reopen (black bars) independently of the large ones while, in the case of D50-5NaCl, most pores reopen simultaneously with the largest ones, which are indicated in red bars. We attribute this difference to the osmotic pressure effect discussed in the following section.

3.6. Discussion on the physical origin of the cooperative pore reopening

In this section, we discuss why a cooperative pore reopening is observed in the samples whose pore solution contains NaCl. We will consider 2 factors successively: (1) osmotic pressure effects which slow the dissolution of small pores surrounding a large one and (2) mechanical shocks caused by the cavitation of a large pore which provoke the reopening of a cluster of pores.

We consider a large spherical pore "LP" of radius R displayed in Fig. 11a surrounded by a spherical shell of PDMS, which itself is surrounded by "dry" air. The shell also contains a small pore "SP". In the presence of salt, in any pore, the drying leads to an increase of the concentration C(NaCl) of the salt in the pore which is inversely proportional to the volume $V(t)$ of this pore as follows: $C(\mathrm{NaCl}) = C_0(\mathrm{NaCl})\cdot V_0/V(t)$, where C_0(NaCl) and V_0 are the salt concentration and pore volume in the initial state, respectively.

As mentioned in Section 3.2, in a diffusion-limited model of pore collapse, the time to full collapse of an individual pore scales with the square of the pore diameter. Hence, a smaller pore should collapse faster than a larger pore. However, this is only expected to be true if we neglect the flow of water between neighboring pores: indeed, if a small pore is very close to a large pore, the flow of water from the large pore to the small pore is expected to significantly slow down the collapse of the small pore. In contrast, if the small pore is closer to the outer edge of the shell, the impact of the large pore on the kinetics of the collapse of the small pore is expected to be more limited. In the next paragraphs, we aim at estimating a characteristic length L_{osm} of influence of the large pore. We define this length of influence as the distance to a large pore below which, because of the presence of the large pore, the salt concentration in the small pore cannot become larger than the solubility.

First, we calculate the water concentration distribution that would prevail in PDMS around the large pore if the shell around the large pore contained no small pore. The thickness of the shell is denoted as L_{dry} and its diffusion coefficient (expressed in $\mathrm{m^2\,s^{-1}}$)

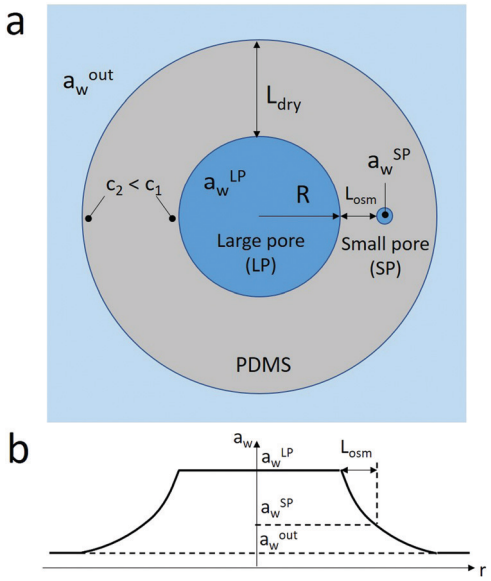

Fig. 11 (a) Model used to estimate the osmotic length L_{osm}: a small spherical pore "SP" with a high concentration of NaCl is located near a large spherical pore "LP" in a PDMS shell of thickness L_{dry}. a_w^{LP}, a_w^{SP} and a_w^{out} are the activities of water in the large pore, small pore and outside medium, respectively; c_1 and c_2 are the water concentrations in PDMS near the large pore and near the border, respectively. The schematic is not drawn to scale, in the sense that the characteristic distance L_{dry} of the large pore to the edge of the sample is, for most pores, much larger than the size of the pore. (b) Corresponding schematic of the radial distribution of water activity in the shell, when neglecting the impact of the small pore "SP".

as D. If we associate a spherical system of coordinates to the large pore with the radial coordinate r, the concentration c of water in the PDMS shell verifies $c(R) = c_1$ and $c(R + L_{dry}) = c_2$. The concentrations c_1 and c_2 are equilibrium water concentrations in PDMS at water activities a_w^{LP} and a_w^{out}, respectively, where a_w^{LP} is the water activity inside the large pore "LP" and a_w^{out} is the water activity outside. We assume ideality of the solution, such that $c_1 = k_D \times a_w^{SP}$ and $c_2 = k_D \times a_w^{out}$, where k_D is a Henry's-type constant. For first-order estimations, literature data[19] show that this assumption is reasonable.

The flow of water through the PDMS shell verifies Fick's law $\underline{j} = -D\underline{\nabla}c$, where $\underline{j}$ (expressed in mol m^{-2} s^{-1}) is the diffusion flux. Combined with the mass balance, Fick's law yields the classical diffusion equation: $\partial c/\partial t = D\Delta c$. We estimate the flow by considering that a steady state has been reached, from which it follows that $\Delta c = 0$. Solving this equation with the aforementioned boundary conditions yields

$$c(r) = \frac{R\cdot(R+L_{dry})}{L_{dry}}\cdot\frac{c_1-c_2}{r} + \frac{1}{L_{dry}}\left(c_2\cdot(R+L_{dry}) - c_1\cdot R\right) \quad (8)$$

As our drying was performed in dry air ($a_w^{out} \approx 0$), we may assume $c_2 \approx 0$, which gives

$$c(r) = c_1\cdot\frac{R}{L_{dry}}\cdot\left(\frac{R+L_{dry}}{r} - 1\right) \quad (9)$$

Now, we consider that a small pore "SP" is located in the shell at the characteristic distance L_{osm} from the surface of the large pore "LP", and that the salt concentration in this small pore is at solubility. The water activity in this small pore is denoted as a_w^{SP}. With the definition of the characteristic distance L_{osm} that we introduced, the small pore must be in thermodynamic equilibrium with the surrounding PDMS.

We assume that the size of the small pore is negligible and that the water concentration distribution in PDMS in the vicinity of the small pore is determined by the large pore and can be obtained using eqn (9), for $r = R + L_{osm}$:

$$c(R+L_{osm}) = c_1\cdot\frac{R}{L_{dry}}\cdot\left(\frac{L_{dry}-L_{osm}}{R+L_{osm}}\right) \quad (10)$$

After taking $c(R + L_{osm}) = k_D \times a_w^{SP}$ and $c_1 = k_D \times a_w^{LP}$, we obtain the equation for L_{osm}:

$$L_{osm} = \left(\frac{R}{a_w^{SP} + a_w^{LP}R/L_{dry}}\right)\left(a_w^{LP} - a_w^{SP}\right) \quad (11)$$

Eqn (11) may be simplified if $R \ll L_{dry}$, which is a strong but reasonable assumption for pores with $R \sim 100$ μm observed in the depth of a rectangular sample with dimensions 10 mm × 10 mm × 0.5 mm (*i.e.* $L_{dry} \sim 250$ μm):

$$L_{osm} \approx R\left(\frac{a_w^{LP}}{a_w^{SP}} - 1\right) \quad (11a)$$

We consider that the NaCl concentration in the small pore reached its solubility: its concentration C_{wt} in g per g of solution is 27 wt%. The NaCl concentration in the large pore is taken to be the one prevailing in sample D300-5NaCl initially, which is equal to 1.5 wt%. Since, assuming ideality, the water activity a_w verifies $a_w = (1 - C_{wt})/(1 - C_{wt} + 2 \times C_{wt} \times M_{H_2O}/M_{NaCl})$, where $M_{H_2O} = 18.0$ g mol^{-1} and $M_{NaCl} = 58.4$ g mol^{-1} are the molar masses of water and NaCl, respectively, the water activities corresponding to those concentrations are $a_w^{SP} = 0.81$ and $a_w^{LP} = 0.99$. The application of eqn (11) (for $R = 100$ μm and $L_{dry} = 250$ μm) and its approximate version (11a) give $L_{osm} = 14.5$ μm and $L_{osm} = 21.6$ μm, respectively. If the small pore "SP" is at a distance larger than L_{osm} from the large pore "LP", it can further shrink. But, in contrast, if it is at a distance smaller than L_{osm} from the large pore "LP", the small pore "SP" will instead gain water and will not go on shrinking until the large pore has significantly shrunk.

In the presence of multiple large pores, as in Fig. 9, the dissolution of small pores between those large pores will be strongly slowed down until the large pore reaches the solubility limit of NaCl, at which point the water in large and small pores will be roughly the same and all osmotic effects will have vanished. Until then, the osmotic effects may maintain the magnitude of the negative pressure in the small pores low enough (in absolute value) to prevent cavitation. Such a mechanism can explain that, in the presence of NaCl, very few small pores reopen before the neighboring large pore has shrunk and is prone to cavitation itself (see Fig. 10c). In the absence of NaCl, there is no osmotic effect between neighboring pores, such that small pores are less impacted by neighboring large

pores and can cavitate before the neighboring large pore has itself shrunk (see Fig. 10b).

The second factor explaining the observation in Section 3.5 of a simultaneous reopening of neighboring pores is based on the recent work of Doinikov *et al.*[22] These authors proposed a model which predicts that the cavitation in a fluid-filled pore under negative pressure may provoke a cavitation in the neighboring pore at the distance of the order of the pore radius. This effect is due to the mechanical shock produced by the cavitation, which may instantly increase the absolute value of the negative pressure inside the neighboring pore. As shown by Vincent *et al.*,[13] for rigid water-filled pores, the cavitation is very sensitive to pressure and even relatively small changes may strongly increase the cavitation probability.

In conclusion, we explain the observed cooperative pore reopening in the presence of NaCl by two effects: the osmotic pressure which tends to equilibrate the negative pressure between the neighboring large and small pores; and the mechanical shock transmission from a pore in which cavitation occurs to its neighbors.

4. Conclusions

In this paper, we investigated the drying of water-filled PDMS sponges with 5% and 30% closed porosity. In these materials, the drying may lead to either a collapsed state with low porosity or the cavitation and reopening of a fraction of the pores. Using optical microscopy and porosity measurements, we showed the influence of the pore diameters and interactions on the result of drying. At pore diameters lower than 20 μm, the majority of pores remain collapsed. This is most likely due to the adhesion of the pore walls and the low probability of the cavitation in a pore with a small volume. Pores with diameters larger than 100 μm tend to reopen after the fluid they contain cavitates. The behavior of pores with diameters ranging from 20 to 100 μm depends on the porosity and drying temperature. In the last sections, we showed evidence of cooperative pore reopening in samples containing NaCl solution inside their pores. We explained this effect by the action of osmotic pressure and the transmission of mechanical shock from a pore in which cavitation occurs to its neighbors.

Our results show the complexity of the drying process for highly deformable materials such as elastomer sponges. Many open questions remain including whether small amounts of water are still present inside the collapsed pores, or what the role of adhesion and mechanical damage of the elastomer matrix in the collapse/reopening process is. To better understand the influence of pore sizes, one needs to perform experiments on monodisperse sponges[23,24] with controllable diameter distributions and porosities. We did not explore porosities larger than 30%, for which we may expect stronger cooperative effects between pores and the existence of collective buckling modes similar to those observed for polymer foams.[25]

Conflicts of interest

The authors declare no competing financial interest.

Acknowledgements

We thank Andrea Aguiar for her help in the formulation of the samples, Ludovic Olanier for help with the fabrication of the hydrostatic balance and Etienne Barthel for fruitful discussions. This work was partially funded by ANR grant MAGELAn <ANR-19-CE06-0024>. We also thank the DIM Respore (http://www.respore.fr/) for having given the last 2 authors the opportunity to meet.

References

1 D. Zhu, S. Handschuh-Wang and X. Zhou, Recent Progress in Fabrication and Application of Polydimethylsiloxane Sponges, *J. Mater. Chem. A*, 2017, **5**(32), 16467–16497, DOI: 10.1039/C7TA04577H.

2 T. Brunet, A. Merlin, B. Mascaro, K. Zimny, J. Leng, O. Poncelet, C. Aristégui and O. Mondain-Monval, Soft 3D Acoustic Metamaterial with Negative Index, *Nat. Mater.*, 2015, **14**(4), 384–388, DOI: 10.1038/nmat4164.

3 Y. Jin, R. Kumar, O. Poncelet, O. Mondain-Monval and T. Brunet, Flat Acoustics with Soft Gradient-Index Metasurfaces, *Nat. Commun.*, 2019, **10**(1), 143, DOI: 10.1038/s41467-018-07990-5.

4 A. Kovalenko, M. Fauquignon, T. Brunet and O. Mondain-Monval, Tuning the Sound Speed in Macroporous Polymers with a Hard or Soft Matrix, *Soft Matter*, 2017, **13**(25), 4526–4532, DOI: 10.1039/C7SM00744B.

5 M. S. Silverstein, PolyHIPEs: Recent Advances in Emulsion-Templated Porous Polymers, *Prog. Polym. Sci.*, 2014, **39**(1), 199–234, DOI: 10.1016/j.progpolymsci.2013.07.003.

6 M. Tebboth, Q. Jiang, A. Kogelbauer and A. Bismarck, Inflatable Elastomeric Macroporous Polymers Synthesized from Medium Internal Phase Emulsion Templates, *ACS Appl. Mater. Interfaces*, 2015, **7**(34), 19243–19250, DOI: 10.1021/acsami.5b05123.

7 A. Turani-i-Belloto, N. Meunier, P. Lopez and J. Leng, Diffusion-Limited Dissolution of Calcium Carbonate in a Hydrogel, *Soft Matter*, 2019, **15**(14), 2942–2949, DOI: 10.1039/C8SM02625D.

8 A. D. Martina, J. G. Hilborn, J. Kiefer, J. L. Hedrick, S. Srinivasan and R. D. Miller, Siloxane Elastomer Foams, in *Polymeric Foams; ACS Symposium Series*, American Chemical Society, 1997, vol. 669, pp. 8–25, DOI: 10.1021/bk-1997-0669.ch002.

9 A. Kovalenko, K. Zimny, B. Mascaro, T. Brunet and O. Mondain-Monval, Tailoring of the Porous Structure of Soft Emulsion-Templated Polymer Materials, *Soft Matter*, 2016, **12**(23), 5154–5163, DOI: 10.1039/C6SM00461J.

10 M. P. Milner, L. Jin and S. B. Hutchens, Creasing in Evaporation-Driven Cavity Collapse, *Soft Matter*, 2017, **13**(38), 6894–6904, DOI: 10.1039/C7SM01258F.

11 S. Cai, K. Bertoldi, H. Wang and Z. Suo, Osmotic Collapse of a Void in an Elastomer: Breathing, Buckling and Creasing, *Soft Matter*, 2010, **6**(22), 5770, DOI: 10.1039/c0sm00451k.
12 M. A. Bruning, M. Costalonga, J. H. Snoeijer and A. Marin, Turning Drops into Bubbles: Cavitation by Vapor Diffusion through Elastic Networks, *Phys. Rev. Lett.*, 2019, **123**(21), 214501, DOI: 10.1103/PhysRevLett.123.214501.
13 O. Vincent, D. A. Sessoms, E. J. Huber, J. Guioth and A. D. Stroock, Drying by Cavitation and Poroelastic Relaxations in Porous Media with Macroscopic Pores Connected by Nanoscale Throats, *Phys. Rev. Lett.*, 2014, **113**(13), 134501, DOI: 10.1103/PhysRevLett.113.134501.
14 T. D. Wheeler and A. D. Stroock, The Transpiration of Water at Negative Pressures in a Synthetic Tree, *Nature*, 2008, **455**(7210), 208–212, DOI: 10.1038/nature07226.
15 C. Fond, Cavitation Criterion for Rubber Materials: A Review of Void-Growth Models, *J. Polym. Sci., Part B: Polym. Phys.*, 2001, **39**(17), 2081–2096, DOI: 10.1002/polb.1183.
16 A. N. Gent and D. A. Tompkins, Surface Energy Effects for Small Holes or Particles in Elastomers, *J. Polym. Sci., Part A-2*, 1969, **7**(9), 1483–1487, DOI: 10.1002/pol.1969.160070904.
17 J. Dollhofer, A. Chiche, V. Muralidharan, C. Creton and C. Y. Hui, Surface Energy Effects for Cavity Growth and Nucleation in an Incompressible Neo-Hookean Material—Modeling and Experiment, *Int. J. Solids Struct.*, 2004, **41**(22), 6111–6127, DOI: 10.1016/j.ijsolstr.2004.04.041.
18 A. M. Stricher, R. G. Rinaldi, C. Barrès, F. Ganachaud and L. Chazeau, How I Met Your Elastomers: From Network Topology to Mechanical Behaviours of Conventional Silicone Materials, *RSC Adv.*, 2015, **5**(66), 53713–53725, DOI: 10.1039/C5RA06965C.
19 S. J. Harley, E. A. Glascoe and R. S. Maxwell, Thermodynamic Study on Dynamic Water Vapor Sorption in Sylgard-184, *J. Phys. Chem. B*, 2012, **116**(48), 14183–14190, DOI: 10.1021/jp305997f.
20 H. C. Cheng and R. Lemlich, Errors in the Measurement of Bubble Size Distribution in Foam, *Ind. Eng. Chem. Fundam.*, 1983, **22**(1), 105–109, DOI: 10.1021/i100009a018.
21 M. Naeimi, A. Karkhaneh, J. Barzin, M. T. Khorasani and A. Ghaffarieh, Novel PDMS-Based Membranes: Sodium Chloride and Glucose Permeability, *J. Appl. Polym. Sci.*, 2013, **127**(5), 3940–3947, DOI: 10.1002/app.37709.
22 A. A. Doinikov, B. Dollet and P. Marmottant, Cavitation in a Liquid-Filled Cavity Surrounded by an Elastic Medium: Intercoupling of Cavitation Events in Neighboring Cavities, *Phys. Rev. E*, 2018, **98**(1), 013108, DOI: 10.1103/PhysRevE.98.013108.
23 A. Giustiniani, P. Guégan, M. Marchand, C. Poulard and W. Drenckhan, Generation of Silicone Poly-HIPEs with Controlled Pore Sizes via Reactive Emulsion Stabilization, *Macromol. Rapid Commun.*, 2016, **37**(18), 1527–1532, DOI: 10.1002/marc.201600281.
24 B. Wang, P. Prinsen, H. Wang, Z. Bai, H. Wang, R. Luque and J. Xuan, Macroporous Materials: Microfluidic Fabrication, Functionalization and Applications, *Chem. Soc. Rev.*, 2017, **46**(3), 855–914, DOI: 10.1039/C5CS00065C.
25 L. J. Gibson and M. F. Ashby, The Mechanics of Three-Dimensional Cellular Materials, *Proc. R. Soc. A*, 1982, **382**(1782), 43–59, DOI: 10.1098/rspa.1982.0088.

